



CHORUS

This is the accepted manuscript made available via CHORUS. The article has been published as:

Strain sensitivity of band gaps of Sn-containing semiconductors

Hong Li, Ivano E. Castelli, Kristian S. Thygesen, and Karsten W. Jacobsen

Phys. Rev. B **91**, 045204 — Published 22 January 2015

DOI: [10.1103/PhysRevB.91.045204](https://doi.org/10.1103/PhysRevB.91.045204)

Strain sensitivity of band gaps of Sn-containing semiconductors

Hong Li, Ivano E. Castelli, Kristian S. Thygesen and Karsten W. Jacobsen*

*Center for Atomic-scale Materials Design, Department of Physics,
Technical University of Denmark, DK - 2800 Kongens Lyngby, Denmark*

Tuning of band gaps of semiconductors is a way to optimize materials for applications within photovoltaics or as photocatalysts. One way to achieve this is through applying strain to the materials. We investigate the effect of strain on a range of Sn containing semiconductors using density functional theory and many-body perturbation theory calculations. We find that the band gaps of bulk Sn oxides with SnO_6 octahedra are highly sensitive to volumetric strain. By applying a small isotropic strain of 2% (-2%), a decrease (increase) of band gaps as large as 0.8 to 1.0 eV are obtained. We attribute the ultrahigh strain sensitivity to the pure Sn *s*-state character of the conduction band edges. Other Sn-containing compounds may show both increasing and decreasing gaps under tensile strain and we show that the behavior can be understood by analyzing role of the Sn *s*-states in both the valence and the conduction bands.

I. INTRODUCTION

The need for more sustainable energy solutions has spawned many efforts in finding materials appropriate for absorption of solar light to be used in either photovoltaics or in solar-to-fuel devices.¹ A key parameter in these materials is the band gap which sets some limits on how efficient the device can be.² The efforts go into discovering entirely new materials but also into optimizing the band gap and band edge positions of known materials in many different ways. The modifications may involve strain,^{3–5} doping,^{6,7} alloying,^{8,9} heterogeneous structuring,¹⁰ surface ligand passivation,¹¹ or atomically thin layering.^{12–14} Strain can be introduced directly in a material by an external applied stress field, but it also often interplays with other modification mechanisms which indirectly modifies the strain. For example the nanostructuring of a material often leads to interface or surface stresses which because of the small scale can have strong strain effects through the entire material. Recently, Yang *et al.* showed how core/shell nanostructures in CdSe/CdTe systems can lead to significant strain-induced band gap modification.¹⁵

In this paper, we study the effect of strain on the band gaps for a series of 14 bulk semiconductors, mainly Sn compounds, using Density Functional Theory (DFT) and many-body perturbation theory within the G_0W_0 approximation. A small strain range from -2% to 2% is applied equally on all the three dimensions. We find that the band gaps of the Sn oxides with SnO_6 octahedra are ultrasensitive to strain. Rotations of the BO_6 octahedra and induced volume changes are investigated in the four primitive perovskite formula cells ($\sqrt{2} \times \sqrt{2} \times 2$) of CaSnO_3 and CaTiO_3 . Finally, we study strain effects in A- and B-site alloys for SrSnO_3 with Ba and Ti, respectively.

II. COMPUTATIONAL METHODOLOGY

We consider the strain dependence of the band gap in fourteen 3D semiconductors, *i.e.*, ten cubic perovskites among ABO_3 (A = Ca, Sr, Ba or Sn, and B = Sn or Ti) and ABl_3 (A = Cs or CH_3NH_3 , and B = Sn or Pb), one rutile SnO_2 , two rhombohedral SnS_2 and SnSe_2 , and one layered perovskite with the Ruddlesden–Popper phase Sr_2SnO_4 . All the structures have octahedral character as part of their geometry. A small strain from -2% to 2% with a step of 0.5% are applied equally in all the three dimensions. Four primitive perovskite formula cells ($\sqrt{2} \times \sqrt{2} \times 2$), are constructed to study CaSnO_3 and CaTiO_3 with rotations of the BO_6 octahedra.

The calculations are all performed using the DFT and many-body perturbation theory code GPAW^{16,17} with the projector augmented wave approximation (PAW) implemented. Bulk lattice relaxations are carried out using the PBEsol exchange-correlation functional.¹⁸ We use a plane-wave cut-off of 800 eV and the Brillouin zones are sampled using a $6 \times 6 \times 6$ Monkhorst-Pack *k*-mesh.¹⁹ The residual force per atom is converged to less than 0.01 eV/Å.

To determine the band structure and band gaps, a denser Γ -centered $10 \times 10 \times 10$ Monkhorst-Pack *k*-point grid is applied. The electronic band gaps are calculated using the exchange-correlation functional GLLB-SC by Gritsenko *et al.*,²⁰ adapted by Kuisma *et al.*²¹ to include the PBEsol correlation for solids (-SC). The GLLB-SC functional include explicit calculation of the derivative discontinuity added to the Kohn-Sham (KS) band gap to obtain the quasiparticle (QP) gap. A number of studies have shown that the GLLB-SC functional at a minimal computational cost gives reasonable band gaps for oxides and other materials in comparison with experiment and many-body perturbation theory.^{22–24} The QP gaps in the G_0W_0 approximation²⁵ are also calculated for BaSnO_3 , and BaTiO_3 using PBE eigenvalues and wavefunctions as input. Considering the balance of accuracy and computer time, two approximations are adopted in the G_0W_0 calculations. One is the use of the Plasmon Pole approximation (PPA) by Godby and Needs for the

dielectric function,²⁶ instead of an explicit treatment of the frequency dependence. This kind of PPA model has been demonstrated to agree well with explicit frequency-dependent method for band gaps.^{27,28} The other approximation is based on the observation that increasing the k-mesh grid leads to only a constant shift of the G_0W_0 QP gaps.²⁵ Thus the G_0W_0 QP gaps are obtained by combining the extrapolation to infinite cut-off energy using a coarse $4 \times 4 \times 4$ k-points and calculation at a low cut-off energy, like 50 eV, for a denser $10 \times 10 \times 10$ k-points.

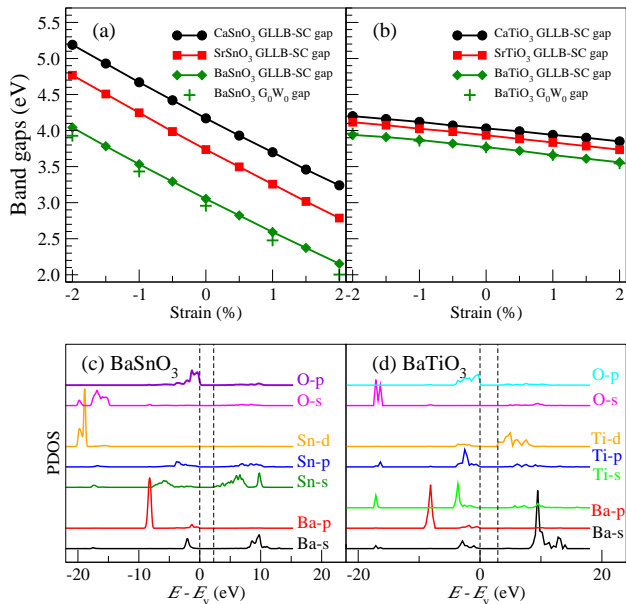


FIG. 1: (a-b) The GLLB-SC and G_0W_0 QP gaps of cubic perovskite ABO_3 ($A = \text{Ca, Sr or Ba}$, and $B = \text{Sn or Ti}$) as a function of strain. (c-d) The PDOS for (c) BaSnO_3 and (d) BaTiO_3 . The gap indicated here is the KS part of the GLLB-SC QP gap with the top of the valence bands set to zero.

III. RESULTS AND DISCUSSIONS

The calculated GLLB-SC QP band gaps of ABO_3 ($A = \text{Ca, Sr or Ba}$, and $B = \text{Ti or Sn}$) as a function of strain are shown in Figs. 1(a) and 1(b) for $B = \text{Sn}$ and $B = \text{Ti}$, respectively. The G_0W_0 QP gaps for BaSnO_3 and BaTiO_3 for some selected strain values are also shown. The agreement between the GLLB-SC and G_0W_0 QP gaps is clearly good with a deviation of only about 0.1 eV. The strain effect on the ASnO_3 series is more remarkable than that of the ATiO_3 ones, and the QP gaps all drop linearly with increasing strains from -2% to 2%. The band gaps decrease (increase) dramatically by 0.90–0.95 eV at a small strain of 2% (-2%) for ASnO_3 , while the drop (increase) for ATiO_3 is only 0.18–0.21 eV at the same strain. In particular, the QP gap of BaSnO_3 drops

from 3.05 to 2.15 eV at a tensile strain of 2%, bringing it into a region relevant for visible light absorption. Our results agree well with recent work on strain effects in SrSnO_3 and BaSnO_3 , where a drop of ~ 1 eV of the band gap with an increase of the volume by $\sim 4 \text{ \AA}^3$ (corresponding to $\sim 2\%$ strain) was found.⁴ We fit the QP gaps with strains using a linearly functional form: $E_g(x) = E_g(0) + k \times x$, where x is the percent of strain. It is interesting to see that each of the ASnO_3 and ATiO_3 series have similar slopes, with values of k from -0.47 to -0.49 and -0.087 to -0.098, respectively. To illuminate the mechanism behind the band gap variation for the two series, we plot the projected density of states (PDOS), for BaSnO_3 and BaTiO_3 in Fig. 1(c) and (d), respectively. The gap indicated here is the KS gap of the GLLB-SC QP gap. We find that all the valence band maxima (VBM) can be mainly attributed to the oxygen (O) p -states, while the conduction band minima (CBM) can be attributed to tin (Sn) s -states and Titanium (Ti) d -states for the ASnO_3 and ATiO_3 series, respectively. The calculations thus suggest that the Sn s -state character plays a major role for the ultra high strain sensitivity.

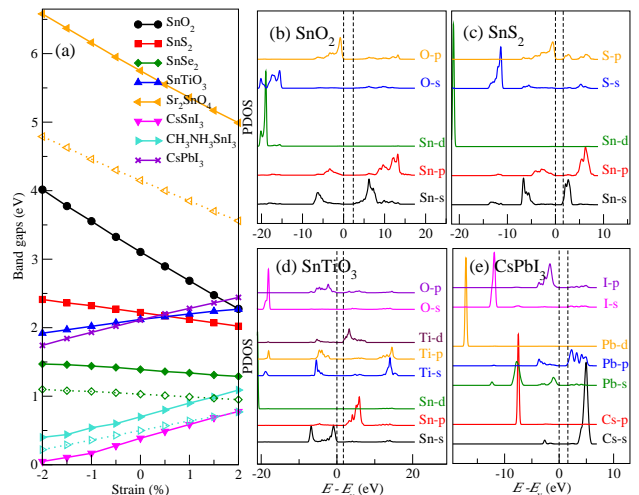


FIG. 2: (a) The GLLB-SC KS (dashed lines and open markers) and QP (solid line and full markers) gaps as a function of strains for a selection of 3D semiconductors. (b-e) The PDOS for (b) SnO_2 , (c) SnS_2 , (d) SnTiO_3 , and (e) CsPbI_3 . The gap appearing in the PDOS is the KS part of the GLLB-SC QP gap and the top of valence band is set to zero.

To investigate more generally the strain sensitivity when Sn is involved, we investigate seven other Sn compounds (SnO_2 , SnS_2 , SnSe_2 , SnTiO_3 , CsSnI_3 , $\text{CH}_3\text{NH}_3\text{SnI}_3$, and Sr_2SnO_4) and also one Pb compound (CsPbI_3). The calculated GLLB-SC KS and QP band gaps as a function of strain are shown in Fig. 2(a). We see that the band gaps can both increase and decrease with strain. For all the systems considered, the strain

shows a combined effect on both the KS gap and the derivative discontinuity. In fact, the changes in the KS and the derivative discontinuity parts of the QP gap due to strain are usually proportional to the contribution they have to the QP gap. The most remarkable variation in the gap is seen for SnO_2 and Sr_2SnO_4 where the variation is of the same order of magnitude as was seen for the ASnO_3 compounds with a band gap drop of about 0.8 eV at a strain of 2%. The sensitivity seems to have the same origin as for the ASnO_3 compounds since the CBM are dominated by Sn s -states for SnO_2 and a combination of Sn and Sr s -states for Sr_2SnO_4 as shown in Fig. 2(b) for the case of SnO_2 .

The compounds SnS_2 and SnSe_2 exhibit a more moderate decrease of the band gap with strain. For these systems the CBM still exhibits some Sn s -state character, however, now mixed with a strong component of S and Se p -states for SnS_2 and SnSe_2 , respectively. This can be seen in the PDOS of SnS_2 in Fig. 2(c). In all the cases with decreasing band gaps, the VBM are dominated by the the anion (O, S or Se) p -states and seem to be play a minor role for the variation observed.

The remaining compounds, SnTiO_3 , CsSnI_3 , $\text{CH}_3\text{NH}_3\text{SnI}_3$, and CsPbI_3 all exhibit an increase in the band gap as a function of strain. In these compounds, the Sn s -states do not come into play at the CBM. For SnTiO_3 the CBM is dominated by Ti d -states (see Fig. 2(d)), while for CsSnI_3 and $\text{CH}_3\text{NH}_3\text{SnI}_3$ the main weight at the CBM comes from the Sn p -states and analogously for CsPbI_3 the Pb p -states.²⁹ However, now the VBM can be attributed to a combination of the Sn/Pb s -states and the anion p -states leading to an increase of the gap with strain.

We verify the role of electronic character of the edge states by calculating the shifts of the edges with strain relative to a common reference taken as the pseudo-Hartree potential close to an atomic core.³⁰ The shifts of the edges at a strain of 2% for BaSnO_3 , SnS_2 , and SnTiO_3 compared to the unstrained situation are given in Table 1. We see that for BaSnO_3 the large drop in band gap comes from the lowering of the CBM which is in this case is dominated by the pure Sn s -states. For SnS_2 the moderate decrease of the band gap is mainly due to the CBM moving down but the effect is smaller than for BaSnO_3 because the CBM is here composed of a mix of Sn s -states and S p -states. For SnTiO_3 the moderate increase of the gap comes from a lowering of the VBM which is associated with a mix of Sn s -states and O p -states. We thus see that in all cases the change in band gap can be understood from a down-shift of the Sn s -states and the effect is particularly large if the Sn s -states are not mixed with other states.

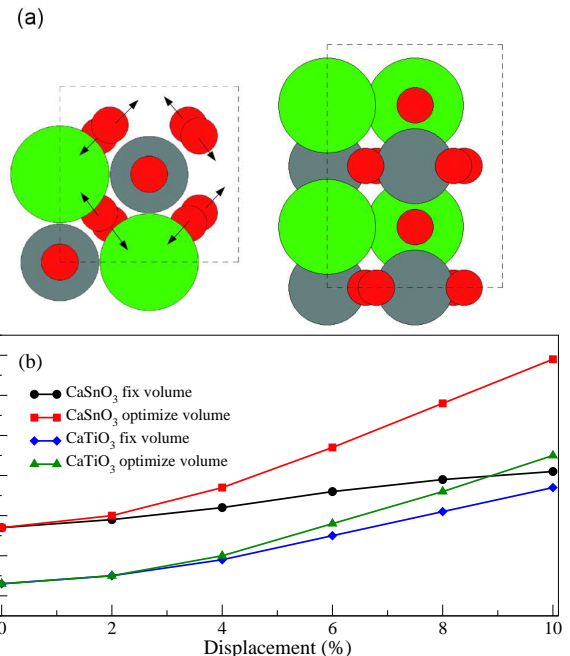


FIG. 3: (a) Illustration of how the rotation of the octahedra in CaSnO_3 and CaTiO_3 are applied (seen from two directions). The displacement measures the movement of one of the oxygen atoms. Green Ball: Ca; Gray Ball: Sn/Ti; Red Ball: O. (b) The calculated GLLB-SC QP gaps as a function of oxygen displacement shown for both fixed and optimized volumes.

TABLE I: The shifts of the band edges (in eV) at 2% strain relative to the unstrained situation for BaSnO_3 , SnS_2 , and SnTiO_3 . The shifts are calculated by taking the pseudo-Hartree potential close to an atomic core as a common reference.

	BaSnO_3	SnS_2	SnTiO_3
CBM	-0.53	-0.17	-0.01
VBM	0.18	-0.03	-0.14

Many perovskites (Pm-3m) commonly occur in an orthorhombic form in nature with space group of Pbnm (*i.e.*, CaSnO_3 and CaTiO_3), with a unit cell which contain four primitive perovskite formula cells ($\sqrt{2} \times \sqrt{2} \times 2$). Tilts and rotations of the BO_6 octahedra take place and give rise to the lattice reconstruction. The calculated GLLB-SC QP gaps for the orthorhombic CaSnO_3 and CaTiO_3 are 4.90 and 4.54 eV, enlarged by 0.73 and 0.51 eV compared to 4.17 and 4.03 eV for the cubic perovskites, respectively.

If the relative positions of the atoms are kept fixed in the reconstructed phase and the lattice parameters are forced to be the ones in the cubic phase, we get GLLB-

SC QP gaps of 4.43 and 4.42 eV for CaSnO_3 and CaTiO_3 , respectively. Thus we see that the tilts and rotations of the internal atom coordinates contribute 0.26 and 0.39 eV to the band gaps, while the reconstruction of the lattice contribute 0.47 and 0.12 eV to the enlargement of the orthorhombic CaSnO_3 and CaTiO_3 , respectively.

To investigate the reconstruction effects on the band gap further, we make a simple model of the reconstruction by just rotating the two oxygen layers of each octahedron gradually in opposite ways around the z-axis (in tetragonal symmetry) as shown in Fig. 3(a). The displacement of the two oxygen layers is along the primitive unit cell vectors in the xy -plane, and we define a displacement parameter as the ratio between the displacement of one of the oxygen atom from its original ideal position and the primitive lattice constant. The GLLB-SC QP gaps of the deformed CaSnO_3 and CaTiO_3 in the $\sqrt{2} \times \sqrt{2} \times 2$ unit cell is shown in Fig. 3(b) for the two different cases of optimized volume and a fixed volume. It is clear to see that the change of volume dominates the increase of the band gap in CaSnO_3 as also found by Singh *et. al.*,⁴ while for the CaTiO_3 the change of band gap is dominated by the rotation of the octahedra. The difference between the two systems arise from the CaSnO_3 having the CBM dominated by the more delocalized Sn s -states which gives a high volume sensitivity,⁴ while the CBM of CaTiO_3 is dominated by Ti d -states where directional bonding plays a significant role.

As seen above, the SrSnO_3 exhibits a very strong strain dependence of the gap. To which extent will such a feature remain if alloying is applied? To study this we consider two examples of 50% substitution of Ba in the A-site (replacing Sr) or Ti in the B-site (replacing Sn). For simplicity, we just take the average lattice parameters of each two perovskites as the equilibrium lattice constant. The GLLB-SC QP gaps as a function of volumetric strain for the two alloys $(\text{Sr}_{0.5}\text{Ba}_{0.5})\text{SnO}_3$ and $\text{Sr}(\text{Sn}_{0.5}\text{Ti}_{0.5})\text{O}_3$ and their PDOS are shown in Fig. 4(a) and (b), respectively. We find that the A-site alloying does not break the strong strain dependence of the band gap, while the substitution at the B-site leads to a much weaker dependence. This dependence supports the previous explanations of the importance of the Sn s -states at the CBM as an indicator of strong strain dependence, because as can be seen in the PDOS in Fig. 4(b), the CBM of the $(\text{Sr}_{0.5}\text{Ba}_{0.5})\text{SnO}_3$ system is dominated by the Sn s -states while in $\text{Sr}(\text{Sn}_{0.5}\text{Ti}_{0.5})\text{O}_3$ the CBM character has changed to Ti d -states. The high strain sensitivity of the band gap of $(\text{Sr}_{0.5}\text{Ba}_{0.5})\text{SnO}_3$ is in good agreement with experimental studies of $(\text{Ba}_{1-x}\text{Sr}_x)\text{SnO}_3$ thin films epitaxially grown on MgO substrates, where tuning the coverage of Sr from $x = 0$ to 1, gradually decreases the out of plane lattice parameter by $\sim 2\%$ and leads to an increase of the band gap by 0.77 eV.⁸

To conclude, the alloying proportion of A-site atom (Ba) in SrSnO_3 tune the band gap not through directly affecting the electronic character of the bands but mainly through the induced change of volume. A similar vol-

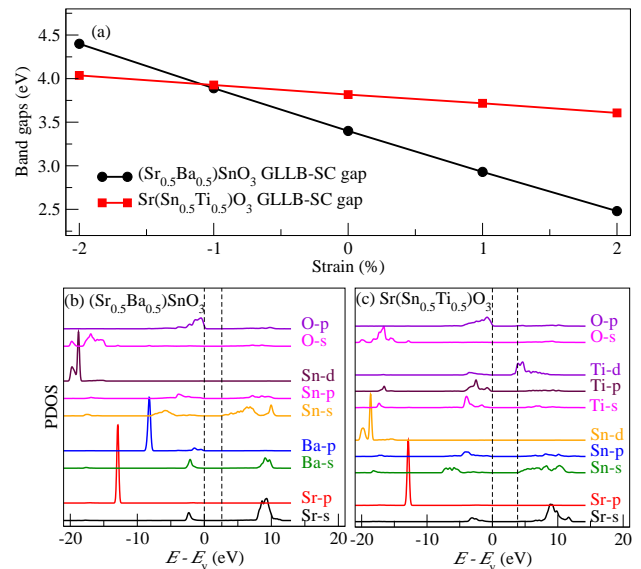


FIG. 4: (a) The GLLB-SC QP gaps with strains for alloys. (b-c) The PDOS for (b) $(\text{Sr}_{0.5}\text{Ba}_{0.5})\text{SnO}_3$ and (c) $\text{Sr}(\text{Sn}_{0.5}\text{Ti}_{0.5})\text{O}_3$. The gap indicated here is the KS part of the GLLB-SC QP gap with the top of valance band set to zero.

ume effect can be seen in ASnO_3 ($A = \text{Ca}, \text{Sr}, \text{and Ba}$) with the increasing volume of the A-site atom. Importantly, this also provides a way of tuning the band gap in the organic perovskites as can be seen by comparing CsSnI_3 and $\text{CH}_3\text{NH}_3\text{SnI}_3$, where the larger A-site molecule CH_3NH_3 leads to a larger volume and therefore a larger gap.³¹

IV. CONCLUSION

We have investigated the possibilities of using strain to modify the band gaps of a range of compounds containing tin based on electronic structure calculations. The increase or decrease in the QP band gap is generated by the variation that the strain induces in both the KS and the derivative discontinuity contributions to the QP gap. The sensitivity of the band gaps to strain is quite different depending on the material and the differences can be systematized by considering the electronic states which play a role for the band edge states. A very high strain sensitivity was observed for the compounds where the CBM states could be attributed to mainly Sn s -states possibly in combination with other s -states. A clear decrease in the band gaps as a function of increasing volumetric strain was thus observed for ASnO_3 ($A = \text{Ca}, \text{Sr}, \text{Ba}$), SnO_2 , and SrSnO_4 . For the cases SnS_2 and SnSe_2 , where the CBM states involve a combination of Sn s -states and anion p -states, a more moderate decrease of the band gap with increasing strain was observed. For the SnTiO_3 and the class of halide perovskites CsSnI_3 ,

$\text{CH}_3\text{NH}_3\text{SnI}_3$, and CsPbI_3 , the effect has the opposite sign, so that a tensile strain leads to an increased band gap, and this behavior can be traced to the VBM now being attributed to a combination of Sn s -states and anion p -states. The large sensitivity to volumetric strain for materials with the CBM dominated by Sn s -states was also confirmed for alloy systems where $(\text{Sr}_{0.5}\text{Ba}_{0.5})\text{SnO}_3$ shows a large decrease of the band gap with increasing strain while $\text{Sr}(\text{Sn}_{0.5}\text{Ti}_{0.5})\text{O}_3$, where the CBM is dominated by Ti d -states, shows a much weaker dependence. Recent experimental investigations of $(\text{Ba}_{1-x}\text{Sr}_x)\text{SnO}_3$ thin films epitaxially grown on MgO substrates confirm the high strain sensitivity of the band gap in this type of

system.

ACKNOWLEDGMENTS

The authors acknowledge support from the Catalysis for Sustainable Energy (CASE) initiative funded by the Danish Ministry of Science, Technology and Innovation and from the Center on Nanostructuring for the Efficient Energy Conversion (CNEEC) at Stanford University, an Energy Frontier Research Center founded by the US Department of Energy, Office of Science, Office of Basic Energy Sciences under award number DE-SC0001060.

-
- * kwj@fysik.dtu.dk
- ¹ M. G. Walter, E. L. Warren, J. R. McKone, S. W. Boettcher, Q. Mi, E. A. Santori, and N. S. Lewis, *Chemical Reviews* **110**, 6446 (2010).
 - ² W. Shockley and H. J. Queisser, *Journal of Applied Physics* **32**, 510 (1961).
 - ³ S. Yang, D. Prendergast, and J. B. Neaton, *Applied Physics Letters* **98**, 152108 (2011).
 - ⁴ D. J. Singh, Q. Xu, and K. P. Ong, *Applied Physics Letters* **104**, 011901 (2014).
 - ⁵ M. Taib, M. Yaakob, A. Chandra, A. K. M. Arof, and M. Yahya, *Advanced Materials Research* **501**, 342 (2012).
 - ⁶ F. Yang, N.-N. Yan, S. Huang, Q. Sun, L.-Z. Zhang, and Y. Yu, *The Journal of Physical Chemistry C* **116**, 9078 (2012).
 - ⁷ F. Wang, C. Di Valentin, and G. Pacchioni, *The Journal of Physical Chemistry C* **116**, 8901 (2012).
 - ⁸ Q. Liu, B. Li, J. Liu, H. Li, Z. Liu, K. Dai, G. Zhu, P. Zhang, F. Chen, and J. Dai, *EPL (Europhysics Letters)* **98**, 47010 (2012).
 - ⁹ N. Alidoust, M. C. Toroker, J. A. Keith, and E. A. Carter, *ChemSusChem* **7**, 195 (2014).
 - ¹⁰ Y. Qu and X. Duan, *Chem. Soc. Rev.* **42**, 2568 (2013).
 - ¹¹ S. Yang, D. Prendergast, and J. B. Neaton, *Nano Letters* **12**, 383 (2012).
 - ¹² Y. Li, Y.-L. Li, C. M. Araujo, W. Luo, and R. Ahuja, *Catal. Sci. Technol.* **3**, 2214 (2013).
 - ¹³ H. L. Zhuang and R. G. Hennig, *Chemistry of Materials* **25**, 3232 (2013).
 - ¹⁴ Y. Yu, S.-Y. Huang, Y. Li, S. N. Steinmann, W. Yang, and L. Cao, *Nano Letters* **14**, 553 (2014).
 - ¹⁵ S. Yang, D. Prendergast, and J. B. Neaton, *Nano Letters* **10**, 3156 (2010).
 - ¹⁶ J. J. Mortensen, L. B. Hansen, and K. W. Jacobsen, *Phys. Rev. B* **71**, 035109 (2005).
 - ¹⁷ J. Enkovaara, C. Rostgaard, J. J. Mortensen, J. Chen, M. Dułak, L. Ferrighi, J. Gavnholt, C. Glinsvad, V. Haikola, H. A. Hansen, H. H. Kristoffersen, M. Kuisma, A. H. Larsen, L. Lehtovaara, M. Ljungberg, O. Lopez-Acevedo, P. G. Moses, J. Ojanen, T. Olsen, V. Petzold, N. A. Romero, J. Stausholm-Møller, M. Strange, G. A. Tritsarlis, M. Vanin, M. Walter, B. Hammer, H. Häkkinen, G. K. H. Madsen, R. M. Nieminen, J. K. Nørskov, M. Puska, T. T. Rantala, J. Schiøtz, K. S. Thygesen, and K. W. Jacobsen, *Journal of Physics: Condensed Matter* **22**, 253202 (2010).
 - ¹⁸ J. P. Perdew, A. Ruzsinszky, G. I. Csonka, O. A. Vydrov, G. E. Scuseria, L. A. Constantin, X. Zhou, and K. Burke, *Phys. Rev. Lett.* **100**, 136406 (2008).
 - ¹⁹ H. J. Monkhorst and J. D. Pack, *Phys. Rev. B* **13**, 5188 (1976).
 - ²⁰ O. Gritsenko, R. van Leeuwen, E. van Lenthe, and E. J. Baerends, *Phys. Rev. A* **51**, 1944 (1995).
 - ²¹ M. Kuisma, J. Ojanen, J. Enkovaara, and T. T. Rantala, *Phys. Rev. B* **82**, 115106 (2010).
 - ²² I. E. Castelli, T. Olsen, S. Datta, D. D. Landis, S. Dahl, K. S. Thygesen, and K. W. Jacobsen, *Energy Environ. Sci.* **5**, 5814 (2012).
 - ²³ I. E. Castelli, J. M. García-Lastra, F. Hüser, K. S. Thygesen, and K. W. Jacobsen, *New Journal of Physics* **15**, 105026 (2013).
 - ²⁴ I. E. Castelli, F. Hüser, M. Pandey, H. Li, K. S. Thygesen, B. Seger, A. Jain, K. A. Persson, G. Ceder, and K. W. Jacobsen, *Advanced Energy Materials*, 1400915 (2014).
 - ²⁵ F. Hüser, T. Olsen, and K. S. Thygesen, *Phys. Rev. B* **87**, 235132 (2013).
 - ²⁶ R. W. Godby and R. J. Needs, *Phys. Rev. Lett.* **62**, 1169 (1989).
 - ²⁷ P. Larson, M. Dvorak, and Z. Wu, *Phys. Rev. B* **88**, 125205 (2013).
 - ²⁸ R. Shaltaf, G.-M. Rignanese, X. Gonze, F. Giustino, and A. Pasquarello, *Phys. Rev. Lett.* **100**, 186401 (2008).
 - ²⁹ We note that spin-orbit coupling has not been included in the calculations presented here. The absolute value of the band gap of CsPbI_3 can therefore be expected to be about 1 eV larger than calculated here³¹.
 - ³⁰ The pseudo-Hartree potential close to an atomic core is calculated as the integral of the s -shaped compensation charge times the pseudo-Hartree potential, i.e., the soft part of the Hartree potential averaged using the s compensation charge as a weight function.
 - ³¹ I. E. Castelli, J. M. Garcia-Lastra, K. S. Thygesen, and K. W. Jacobsen, *APL Materials* **2**, 081514 (2014).